Thermodynamic Stability of Archaeal Histones†

Wen-tyng Li,‡ Rowan A. Grayling,‡ Kathleen Sandman,‡ Steve Edmondson,§ John W. Shriver,*,§ and John N. Reeve*,‡

Department of Microbiology, The Ohio State University, 484 West 12th Avenue, Columbus, Ohio 43210-1292, and Department of Medical Biochemistry, School of Medicine, Southern Illinois University, Carbondale, Illinois 62901-4413

Received December 8, 1997; Revised Manuscript Received March 27, 1998

ABSTRACT: The temperature, salt, and pH dependencies of unfolding of four recombinant (r) archaeal histones (rHFoB from the mesophile *Methanobacterium formicicum*, and rHMfA, rHMfB, and rHPyA1 from the hyperthermophiles *Methanothermus fervidus* and *Pyrococcus* strain GB-3a) have been determined by circular dichroism spectroscopy (CD) and differential scanning calorimetry (DSC). The thermal unfolding of these proteins is >90% reversible, with concentration-dependent apparent T_m values and asymmetric unfolding transitions that are fit well by a two-state unfolding model in which a histone dimer unfolds to two random coil monomers. rHPyA1 dimers are stable in the absence of salt, whereas rHMfA, rHMfB, and rHFoB dimers unfold at 20 °C and pH 2 in solutions containing <200 mM, <400 mM, and <1.5 M KCl, respectively. rHMfA, rHMfB, and rHFoB also experience significant cold denaturation in low salt concentrations and at low pH. The midpoint of thermal unfolding of a 1 M protein solution ($T°$ value) and the temperature dependency of the free energy of unfolding have been established for each histone, and both parameters correlate with the growth temperature of the originating archaeon. The changes in heat capacity upon unfolding are similar for the four histones, indicating that enhanced thermostability is not obtained by altering the curvature of the stability curve. Rather, the stability curves for the histones from the hyperthermophiles are displaced vertically to higher energies and laterally to higher T_{max} values relative to the stability curve for rHFoB. The maximal free energies of unfolding for rHFoB, rHMfA, rHMfB, and rHPyA1 are 7.2, 15.5, 14.6, and 17.2 kcal/mol at 32, 35, 40, and 44 °C, respectively. $T°$ values for rHFoB, rHMfA, rHMfB, and rHPyA1 are 75, 104, 113, and 114 °C, respectively, at pH 5 in 0.2 M KCl. Structural features within the conserved histone fold that might confer these stability differences are discussed.

Comparing the structure and stability of related proteins from species that grow at different temperatures is an established approach for relating structure to thermal stability, and in this regard, the archaeal histones appear to offer an attractive experimental system. They are very small, containing only 66−69 amino acid residues, and 18 sequences are already available from mesophilic, thermophilic, and hyperthermophilic *Archaea* that exhibit 65−85% sequence identity [Figure 1 (*1*)]. The histone fold, namely, a long α-helix flanked and separated from two shorter α-helices by short β-strand loops (*2*, *3*), has been firmly established for the recombinant (r) versions of HMfB from the hyperthermophile *Methanothermus fervidus* (*4*) and for rHFoB from the mesophile *Methanobacterium formicicum* (*5*), and it appears likely that all archaeal histones form this fold (*1*). Archaeal histones share a common ancestry with the eukaryal nucleosome core histones (*6*, *7*), and consistent with this, they are dimers in solution (*8*). However, whereas the eukaryal histones form only (H2A−H2B) and (H3−H4) heterodimers, the archaeal histones form both homodimers and heterodimers (*1*, *9*). Expression of an archaeal histone-encoding gene in *Escherichia coli* therefore results in the synthesis of recombinant homodimers which can be prepared in large amounts with the wild-type sequence or with desired amino acid substitutions (*10*).

Here we present detailed characterizations of the stabilities of four archaeal histones, in terms of temperature, salt, and pH: rHFoB, rHMfA, rHMfB, and rHPyA1, the recombinant versions of histones from *M. formicicum*, *Me. fervidus*, and *Pyrococcus* strain GB-3a, *Archaea* that grow optimally at 43, 83, and 95 °C, respectively (*6*, *11*, *12*). These proteins unfold reversibly; therefore, it was possible to define their stabilities accurately in terms of the thermodynamics of unfolding, and a simple two-state model in which a dimer unfolds to two random coil chains is shown to provide an excellent fit of the thermal unfolding data. This model has been used to extract the free energies of unfolding, changes in heat capacity (ΔC_p), and the thermal stabilities of the four histones in terms of $T°$. The results obtained demonstrate that the recombinant histones have inherently different stabilities that correlate with the growth temperature of the archaeon from which the histone-encoding gene was cloned.

MATERIALS AND METHODS

Protein Purifications. (A) rHMfA and rHMfB. rHMfA and rHMfB were purified from *E. coli* JM105 strains, as previously described (*4*, *9*, *10*).

† This work was supported by NIH Grants GM53185 (J.N.R.) and GM49686 (J.W.S.).

* Corresponding authors. J.N.R. e-mail: reeve.2@osu.edu. J.W.S. e-mail: jshriver@som.siu.edu.

‡ The Ohio State University.

§ Southern Illinois University.

S0006-2960(97)03006-7 CCC: $15.00
Published on Web 07/07/1998

```
                        |--helix1---|          |-----------helix2----------|          |--helix3--|
                        1         10        20         30        40        50        60        69
HMfA      (83)  MGELPIAPIGRIIKNAGAERVSDDARIALAKVLEEMGEEIASEAVKLAKHAGRKTIKAEDIELARKMFK*
HMfB      (83)  M-ELPIAPIGRIIKDAGAERVSDDARITLAKILEEMGRDIASEAIKLARHAGRKTIKAEDIELAVRRFKK*
HFoB      (43)  M-ELPIAPIGRIIKNAGAERVSDDAREALAKALEEKGETIATEAVKLAKHAGRKTVKASDVELAVKRL*
HPyA1     (95)  MGELPIAPVDRLIRKAGAERVSEEAAKILAEYLEEYAIEVSKKAVEFARHAGRKTVKAEDIKLAIKS*
HFoA1     (43)  MAELPIAPVGRIIKNAGAPRVSDDARDALAKVLEEMGEGIAAEAVKLAKHAGRKTVKASDIEMAVKAA*
HFoA2     (43)  MAELPIAPVGRIIKNAGAQRISDDAKEALAKALEENGEELAKKAVELAKHAGRKTVKAEDIEMAVKSA*
HPyA2     (95)  MAELPIAPVDRLIRKAGAQRVSEQAAKLLAEHLEEKALEIARKAVDLAKHAGRKTVKAEDIKLAIRS*
HMtA1     (65)  MAELPIAPVGRIIKNAGAQRISDDAREALAKILEEKGEEIAKEAVKLAKHAGRKTVKASDIELAAKKL*
HMtA2     (65)  MAELPIAPVGRIIKNAGAQRISDDAKEALAKALEEMGEEISRKAVELAKHAGRKTVKATDIEMAAKQL*
HMtB      (65)  M-ELPIAPIGRIIKNAGAEIVSDDAREALAKVLEAKGEEIAENAVKLAKHAGRKTVKASDIELAVKRM*
HAN1A1    (75)  MAELPIAPIDRLIRKAGAERVSEDAAKALAEYLEEYAIEVGKKATEFARHAGRKTVKAEDVRLAVKA*
HAfA      (83)  MAELPMAPVDRLIRKAGAERVSADAVEKMVEVLEDYAITVAKKAVEIAKHSGRKTVTADDIKLALSM*
HAfB      (83)  M-ELPLAPVERLLRKAGASRVSEDAKVELAKAIEEYAMQIGKKAAELAKHAGRKTVKVDDIKLALREL*
MJ0168    (85)  MAELPVAPFERILKKAGAERVSEAAAEYLAEAVEEIALEIAKEAVELAKHAKRKTVKVEDIKLALKK*
MJ0932    (85)  MAELPVAPFERILKKAGAERVSRAAAEYLAEAVEEIALEIAKEAVELAKHAKRKTVKVEDIKLALKQ*
MJ1258    (85)  MAELPVAPCVRILKKAGAQRVSEAAGKYFAEALEEIALEIARKSVDLAKHAKRKTVKVEDVKAALRG*
MJECL17   (85)  MAELPVAPFVRILKKDGAERVSRAAAEYFAEAIEDLALEIAKEAVDLAKHAKRKTVKVEDVKLALKK*
MJECL29   (85)  MTELPVAPFERILKKVGAERVSRAAAEYLAEAFEEIALEIAKEAVDLAKHAKRKTVKVEDIKLALKK*
```

histone	HMfA	HMfB	HFoB	HPyA1	HFoA1	HFoA2	HPyA2	HMtA1	HMtA2	HMtB	HANA1	HAfA	HAfB	MJ 0168	MJ 0932	MJ 1258	MJEC L17	MJEC L29
charge	1	3	2	1	1	0	4	3	1	1	1	0	3	2	1	5	2	2
isoele.pt.	9.2	10.4	10.0	9.1	9.2	7.5	10.6	10.2	9.2	9.2	9.2	7.5	10.2	9.8	9.1	10.4	9.8	9.8
ala	12	11	13	12	16	15	14	14	14	13	15	12	12	15	15	14	14	13
cys	0	0	0	0	0	0	0	0	0	0	0	0	0	0	0	1	0	0
asp	3	5	3	2	4	3	3	3	3	3	3	5	3	1	1	2	4	2
glu	9	7	8	10	6	9	7	8	8	8	9	6	8	11	11	7	8	10
phe	1	1	0	1	0	0	0	0	0	0	1	0	0	1	1	1	2	2
gly	5	4	4	3	5	4	2	4	4	4	3	2	3	1	1	3	1	1
his	1	1	1	1	1	1	2	1	1	1	1	1	1	1	1	1	1	1
ile	8	10	5	6	5	5	5	7	6	7	4	4	3	4	4	3	3	4
lys	8	7	8	8	7	9	8	10	8	8	7	7	9	10	9	9	10	10
leu	5	5	6	5	4	5	8	6	5	5	5	5	9	7	7	6	7	7
met	2	2	1	1	3	2	1	1	3	2	1	4	2	1	1	1	1	1
asn	1	0	1	0	1	2	0	1	1	2	0	0	0	0	0	0	0	0
pro	2	2	2	2	3	2	2	2	2	2	2	2	2	2	2	2	2	2
gln	0	0	0	0	0	1	2	1	2	0	0	0	1	0	1	1	0	0
arg	5	8	5	5	4	3	6	4	4	4	6	4	5	4	4	5	4	4
ser	2	2	2	3	2	2	2	2	2	2	1	3	2	1	1	2	1	1
thr	1	2	3	1	1	1	1	1	2	1	2	3	1	1	1	1	1	2
val	3	2	5	5	6	4	4	3	3	5	5	8	5	6	6	7	7	6
trp	0	0	0	0	0	0	0	0	0	0	0	0	0	0	0	0	0	0
tyr	0	0	0	2	0	0	0	0	0	0	2	1	1	1	1	1	1	1

FIGURE 1: Alignment and an amino acid composition tabulation of all archaeal histone sequences (*1*). The optimum growth temperature of the archaeon from which the corresponding histone originates is indicated by the figure in parentheses (degrees Celsius). The predicted net charge and isoelectric points are included for each histone for comparative purposes.

(B) rHFoB. The *hfoB* gene (*12*) was subcloned into the expression vector pALTER-Ex1 (Promega Corp., Madison, WI), placing *hfoB* transcription under the control of a *tac* promoter. *E. coli* JM105 cultures carrying this plasmid, designated pKS406, were grown to an OD_{600} of ~0.4 in Luria-Bertani medium (*13*) that contained 12.5 μg of tetracycline/mL, and isopropyl D-thiogalactopyranoside was then added (final concentration of 400 μM) to induce rHFoB synthesis. Incubation was continued for 3 h at 37 °C; the cells were harvested, and rHFoB preparations were purified as previously described (*12*), except that the buffer used was 50 mM 2-(*N*-morpholino)ethanesulfonic acid (MES, pH 6).

(C) rHPyA1. The *hpyA1* gene was PCR-amplified from pKS392 (*11*) using 5′-AAAGGATCCCCCATAAATAACTG-3′ and universal sequencing primer no. 1211 (New England Biolabs, Beverly, MA) as primers. The amplified DNA and the expression vector pRAT4 (*14*) were digested with *Bam*HI and *Hin*dIII, mixed, ligated, and used to transform *E. coli* DH5α to ampicillin resistance. The resulting plasmid, pKS471, was transformed into *E. coli* B834 (Novagen, Madison, WI), and rHPyA1 synthesis was induced and rHPyA1 purified from the transformed strain with procedures identical to those used for rHMfB, except that the buffer was 50 mM MES (pH 6).

Protein Concentration Measurements. rHMfA, rHMfB, and rHFoB do not contain tryptophan or tyrosine residues, and protein concentrations were therefore determined by amino acid analyses. Approximate protein concentrations were established by Bradford assays (*15*), and solutions were then diluted to ~1 mg/mL. Following dialysis against 0.5 M ammonium acetate (pH 7) in a Microdialysis System (Gibco-BRL Life Technologies, Gaithersburg, MD), the protein was dried under vacuum, washed with deionized water, purged with N_2 to remove residual ammonium acetate, and hydrolyzed in a Waters Picotag workstation by incubation at 110 °C in 6 N HCl for 24 h (Millipore Corp., Milford, MA). The hydrolyzed material was re-dried twice in water/0.25 M sodium acetate/methanol/triethylamine (1:1:2:1) and derivatized in water/phenyl isothiocyanate/methanol/triethylamine (1:1:6.3:1), and the amino acid content was deter-

mined by using a Waters Picotag amino acid analysis system. All protein concentrations are stated in terms of monomers, and the values reported are the averages of three separate determinations that varied by <10%.

Circular Dichroism (CD). CD spectra of solutions ranging from 1.8 to 5 μM protein were obtained using an Aviv 62DS spectropolarimeter (AVIV, Lakewood, NJ) with a 10 mm path length cylindrical cell. CD measurements at 222 nm were taken at 1 °C intervals from 0 to 99 °C using an averaging time of 60 s. The temperature of the sample was computer controlled to within 0.2 °C. Baseline measurements on deionized water were subtracted from the experimental data. The dependencies of CD intensities on KCl concentration and pH were determined at 20 °C, using a 1 mm path length cylindrical cell and averaging times of 5 or 10 s.

Differential Scanning Calorimetry (DSC). The thermal unfolding of proteins in 0.2 and 1 M KCl, at different pHs, was measured using a MicroCal MC2 calorimeter (Microcal, Northampton, MA) at a scan rate of 1 °C/min. The buffers used to obtain pHs of 2−4, 5, 6, and 7.5 were 25 mM glycine, acetate, MES, and phosphate, respectively. Protein solutions were dialyzed overnight against several changes of the appropriate buffer, and the reference cell contained an aliquot of the final dialysis buffer. Samples were not degassed but were heated three times by scanning to 45 °C, followed by rapid cooling, and N_2 (~30 psi) was introduced into the cells to minimize degassing during scanning. Scans were repeated on all samples to monitor reversibility. The raw data were converted to excess heat capacity (C_p in calories per degree Celsius per mole) by dividing the data points by the scan rate and the total concentration of protein monomers. Scans of the dialysis buffer provided baseline data that were subtracted from protein scans. Protein concentrations ranged from 150 to 500 μM.

Analysis of Dimer Unfolding Data. Cross-linking and NMR studies (*4*, *5*, *8*) have demonstrated that rHMfB and rHFoB are dimers in solution, and the data generated are best fit by a two-state model in which a dimer unfolds to give two random coil monomers, i.e., D → 2M. This model assumes that all intermediates, e.g., folded monomers and higher-order oligomers, are negligibly populated and therefore thermodynamically insignificant, assumptions that appear to be validated by the excellent quality of the fit to the data. The total concentration of protein, $[P_t]$, is expressed in terms of monomer chains such that

$$[P_t] = [M] + 2[D] \tag{1}$$

where [M] and [D] are the concentrations of monomer and dimer, respectively. The equilibrium constant for unfolding is given by

$$K = \frac{[M]^2}{[D]} = \frac{[M]^2}{{}^1/_2([P_t] - [M])} = \frac{2[M]^2}{[P_t] - [M]} \tag{2}$$

Solving for [M] provides an expression for the concentration of unfolded monomer in terms of the equilibrium constant K and the total protein concentration (*16*):

$$[M] = \frac{-K}{4} + \frac{K}{4}\left(1 + \frac{8[P_t]}{K}\right)^{0.5} \tag{3}$$

The equilibrium constant is determined by the free energy of unfolding of the dimer at any temperature T:

$$K = e\left(-\frac{\Delta G°(T)}{RT}\right) \tag{4}$$

K is defined here as a true equilibrium constant that is independent of concentration, whereas the alternative treatment of Thompson et al. (*17*) defines K as a concentration-dependent stability constant.

The free (or Gibbs) energy of unfolding of the dimer is given by the modified Gibbs−Helmholtz equation:

$$\Delta G°(T) = \Delta H°(T°)\left(\frac{T° - T}{T}\right) - (T° - T)\Delta C_p + T\Delta C_p \ln\left(\frac{T°}{T}\right) \tag{5}$$

where $\Delta H°(T°)$ is the standard state enthalpy of unfolding of the dimer at $T°$, ΔC_p is the change in heat capacity for unfolding of the dimer, and $T°$ is the temperature at which the free energy of unfolding of a 1 M protein solution is zero (the standard state is defined as 1 M total protein). The $T°$ so defined is identical to that obtained from the alternative treatment (*17*), and is not the T_m. The progress of the unfolding reaction as a function of temperature is given by the temperature dependency of the fraction of protein which exists as unfolded monomer:

$$\alpha(T) = \frac{[M]}{2[D] + [M]} = \frac{[M]}{[P_t]} = \frac{(K[D])^{0.5}}{[P_t]} \tag{6}$$

$\alpha(T)$ defines the temperature dependency of a spectroscopic signal that is sensitive to the folded state of the protein, such as the CD intensity at 222 nm (*18*). A DSC endotherm is proportional to the partial derivative of α with respect to T (*19*, *20*), such that the excess heat capacity is given by

$$C_p(T) = [\Delta H° - \Delta C_p(T° - T)]\frac{\partial \alpha}{\partial T} \tag{7}$$

The derivative can be calculated numerically at any temperature. The parameters $\Delta H°$, $T°$, and ΔC_p are obtained by nonlinear regression to fit either eq 6 to CD data or eq 7 to DSC data. It is common to define the temperature of the midpoint of the transition as T_m, but for a dimer, this is not the same as the maximum of the DSC endotherm or the inflection point of the progress curve due to the asymmetry of the transition (*21*). By definition, $\alpha(T)$ is equal to 0.5 at the T_m, and since

$$K = \frac{2\alpha^2[P_t]}{1 - \alpha} \tag{8}$$

the standard state free energy of unfolding, $\Delta G°$, is given by $-RT_m \ln[P_t]$ (not zero) at the T_m (*16*).

Note that the calorimetric enthalpy can be specified per mole of monomer or dimer, whereas the van't Hoff enthalpy intrinsically has the units of energy per mole of cooperative unit (*22*), i.e., of dimer here. Since ΔC_p is obtained from the temperature dependency of ΔH_{vh}, ΔC_p is defined for the cooperative unit, i.e., the dimer in this case. As protein concentrations are defined here in terms of total monomers,

the excess heat capacities observed in DSC experiments are expressed in terms of the total concentration of monomers, i.e., calories per degree Celsius per mole of monomer, and the calorimetric enthalpies (the areas under the endotherms) therefore have units of kilocalories per mole of monomer. In practice, the van't Hoff enthalpy is obtained from the temperature dependency of the equilibrium constant for unfolding and is obtained from the DSC data by nonlinear regression using eq 7 with a scaling factor β:

$$C_p(T) = [\Delta H^\circ - \Delta C_p(T^\circ - T)] \frac{\partial \alpha}{\partial T} \beta \qquad (9)$$

where β is the calorimetric to van't Hoff enthalpy ratio:

$$\beta = \frac{\Delta H_{cal}}{\Delta H_{vh}} \qquad (10)$$

A ratio of 0.5 would indicate a two-state unfolding reaction in which the unfolding cooperative unit is twice the size of the monomer (*23*). By comparison, the treatment of Thompson et al. (*17*) differs in basing all thermodynamic parameters on the monomer, and the treatment of Steif et al. (*16*) specifies all thermodynamic parameters, including the excess heat capacity and the calorimetric enthalpy, in terms of the dimer. Thus, a two-state, dimer to monomer unfolding reaction using the Steif et al. (*16*) treatment has a $\Delta H_{cal}/\Delta H_{vh}$ ratio of 1. The treatment used here, ΔH_{cal} expressed in terms of the monomer and ΔH_{vh} and ΔC_p in terms of the cooperative unit, i.e., the dimer, is preferred because it emphasizes the fact that the thermal dependence of the unfolding progress is twice that expected (*22*).

RESULTS

Salt Dependency and Thermostability. Circular dichroism (CD) measurements revealed that unfolding of rHMfA, rHMfB, and rHFoB was salt-dependent at low pH. rHMfA was almost fully unfolded in the absence of KCl at pH 2 and 20 °C but had ~50% folded structure in 50 mM KCl, whereas rHMfB and rHFoB were fully unfolded below 100 and 800 mM KCl, respectively (Figure 2A). rHMfA, rHMfB, and rHFoB required approximately 200 mM, 400 mM, and 1.5 M KCl, respectively, for maximal folding at pH 2 and 20 °C, whereas rHPyA1, the histone from the most hyperthermophilic archaeon, was fully folded from 0 to 1 M KCl (Figure 2A). Increasing the salt concentration increased apparent high-temperature transition midpoints (T_m) and decreased cold denaturation transition temperatures (Figure 2B). The T_m values of rHMfA, rHMfB, and rHPyA1 were so high in 1 M KCl that complete CD transitions and DSC endotherms could not be fully observed with the available instruments, and most of the data for these proteins were therefore collected in 0.2 M KCl. Data from complete CD transitions and DSC endotherms were collected for rHFoB in both 0.2 and 1 M KCl.

Reversibility. To extract thermodynamic parameters, thermal unfolding reactions must be reversible and the unfolding of rHMfA and rHMfB in 0.2 M KCl from pH 3 to 6, of rHPyA1 in 0.2 M KCl from pH 4 to 7.5, and of rHFoB in 1 M KCl from pH 3 to 6 was shown to be reversible. As illustrated in Figure 3A, the areas under the endotherms of consecutive DSC scans of the same rHMfA preparation indicate that rHMfA folding−unfolding was ~94% reversible after heating to 100 °C. This level of reversibility is adequate for thermodynamic analyses, and this or higher levels of reversible unfolding were observed for all four archaeal histones within the pH ranges listed above. Protein aggregation, especially at the high protein concentrations required for DSC, reduced reversibility at lower pHs.

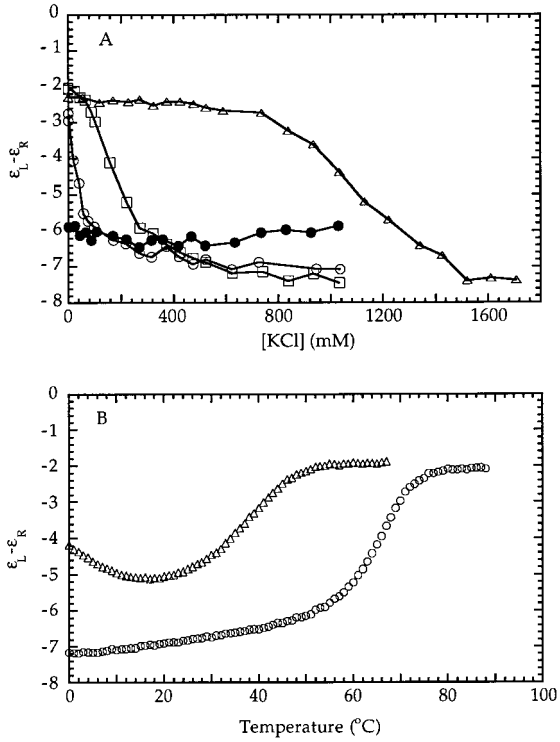

FIGURE 2: (A) Dependency of the extent of folding of rHMfA, rHMfB, rHPyA1, and rHFoB on KCl concentration as measured by CD at 222 nm. Data were collected from 16 μM rHMfA (○), 23 μM rHMfB (□), 15 μM rHPyA1 (●), and 15 μM rHFoB (△) solutions (moles of monomer) at pH 2 in 50 mM glycine buffer at 20 °C. (B) Thermal unfolding of rHMfA followed by CD in 0.2 (△) and 1 M (○) KCl at pH 2 in 25 mM glycine buffer. Protein concentrations were 3.3 and 2.7 μM total monomer in 0.2 and 1.0 M KCl, respectively.

Dimer Unfolding Model. Consistent with the cross-linking and NMR studies that have demonstrated that the archaeal histones are dimers in solution (*4*, *5*, *8*), the DSC endotherms for unfolding showed pronounced asymmetries with greater excess heat capacity below than above the maxima (Figure 3A). Asymmetries were also present in the CD thermal unfolding data, with a gradual change in CD intensity prior to the T_m being followed by a rapid completion of the transition (Figure 3B). Attempts to fit the DSC data for rHMfA as a two-state unfolding of a monomer revealed that the widths of the endotherms were significantly narrower than expected given the intensities, i.e., $\Delta H_{cal}/\Delta H_{vh}$ ratios were <1. A ΔH_{vh} which is greater than ΔH_{cal} indicates that the unfolding cooperative unit is larger than the molecular weight of the monomer, and therefore that the protein exists in solution as a dimer or higher-order oligomer. Equations 6 and 7 (Materials and Methods) indicate that the midpoint of the unfolding transition for a dimer should be concentration-dependent (*16*−*18*), and as predicted, the thermal unfolding of a 153 μM solution of rHMfA followed by DSC gave a T_m of 83 °C (Figure 3A) whereas a 2.3 μM solution

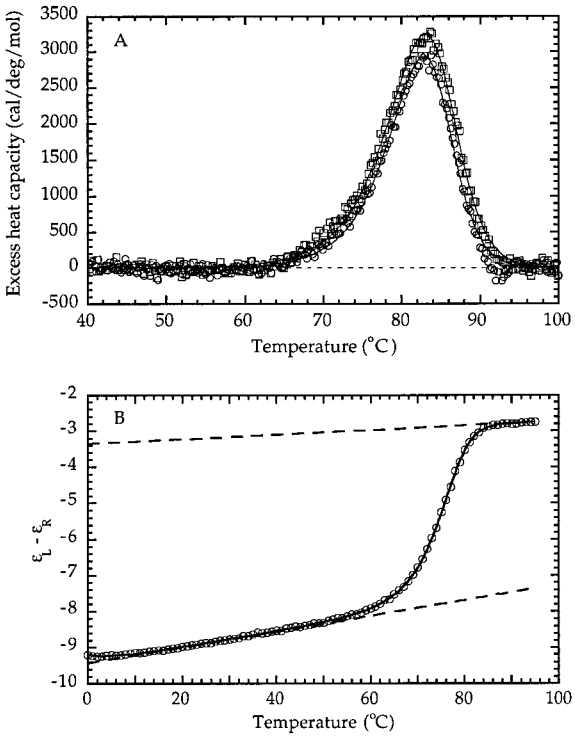

FIGURE 3: (A) Thermal unfolding of rHMfA monitored by DSC. The extent of reversibility of unfolding demonstrated by consecutive DSC scans of the same 153 μM solution (total monomer) in 0.2 M KCl at pH 4 in 25 mM glycine buffer. The endotherms have areas, i.e., ΔH_{cal}, of 41.3 (□) and 38.7 (○) kcal/mol, indicating 93.7% reversibility. A nonlinear least-squares fit (smooth curve) of the first scan (□), based on the two-state dimer to two random coils model, produced a $\Delta H°_{vh}$ of 160 kcal/mol, a $T°$ of 97.5 °C, and a T_m of 83 °C. (B) Thermal unfolding of rHMfA monitored by CD. The buffer and salt conditions were the same as in panel A but with a monomer concentration of 2.3 μM. A nonlinear least-squares fit (smooth curve), based on the two-state dimer to random coils model, produced a $\Delta H°_{vh}$ of 161 kcal/mol, a $T°$ of 100.2 °C, a T_m of 74 °C, and a ΔC_p of 2225 cal deg^{-1} (mol of dimer)$^{-1}$. The baselines for native and unfolded protein obtained from the fit are indicated by dashed lines.

followed by CD had a T_m of 75 °C (Figure 3B). This difference was not assay- or instrument-dependent as CD data alone demonstrated a monotonic increase in the apparent T_m for unfolding with increasing protein concentration (Figure 4).

On the basis of these observations, it appeared that the thermal unfolding of the archaeal histones might be defined by a simple two-state model, a dimer unfolding directly to two random coils, and this model did indeed give excellent nonlinear least-squares fits to both the DSC and CD data. The smooth curves in panels A and B of Figure 3 are fits based on this model, and very similar $\Delta H°_{vh}$ values, 158 and 161 kcal/mol of dimer, were obtained from these fits of the DSC and CD data, respectively. In addition, there is also excellent agreement between the experimental data and the concentration dependency of the apparent T_m predicted by the model using the parameters obtained from independent fits of the CD and DSC data. The predicted T_m values, shown as a smooth curve in Figure 4, fit the experimentally determined T_m values to within 1 °C over the full experimental range of protein concentrations (0.85−153 μM). For comparative purposes, the concentration dependency of apparent T_m values of oligomeric proteins can be circumvented by considering $T°$ values, a fitted parameter that

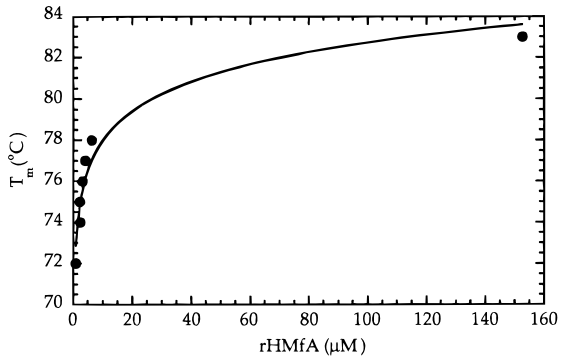

FIGURE 4: Protein concentration dependency of the apparent T_m of rHMfA at pH 4 in 25 mM glycine buffer that contained 0.2 M KCl. The estimated error in the T_m is <1 °C. Note that the smooth curve through the data points is not a fit but corresponds to a $T°$ of 98.8 °C, a ΔH of 159.5 kcal/mol, and a ΔC_p equal to 2225 cal deg^{-1} (mol of dimer)$^{-1}$, the average values obtained for these parameters from independent fits of the DSC and CD data in panels A and B of Figure 3.

represents the T_m of a 1 M solution (see Data Analysis). The $T°$ values obtained for rHMfA from fitting these DSC and CD data are 97.6 and 100.2 °C, respectively. This close agreement of $T°$ values obtained by two independent methods, at different protein concentrations, adds further strong support to the validity of the two-state, dimer unfolding model.

Despite these agreements between the model and data, the $\Delta H_{cal}/\Delta H_{vh}$ ratios from fits of the data deviate from 0.5, the ratio predicted by the model. For example, a ratio of 0.26 is obtained from the fit of the data in Figure 3B. As rHMfA is only ~80% folded at pH 4 in 0.2 M KCl (Figure 5A), the predicted $\Delta H_{cal}/\Delta H_{vh}$ ratio is actually 0.4 rather than 0.5, but this is still significantly larger than 0.26. Inaccuracies in defining DSC post-transition baselines, a technical problem inherent in working with very stable proteins from hyperthermophiles (*24*), are likely to have caused these discrepancies. Sigmoidal transitions in the baselines were removed from the experimental data as described (*24*); however, errors in the ΔH_{cal} were likely when the baseline information available above the transition was insufficient for a reliable fit. As the ΔH_{cal} values exhibited greater fluctuations and the ΔH_{vh} values obtained by DSC and CD were generally consistent with each other, less emphasis was placed on the calorimetric ΔH values.

Thermodynamics of Unfolding. (A) rHMfA. Complete thermal unfolding transitions of rHMfA were followed by CD and DSC in 0.2 M KCl from pH 3 to 6. Representative CD thermal melts at different pHs are shown in Figure 5A, and the thermodynamic parameters derived from nonlinear least-squares fits of the CD and DSC data are listed in Table 1. The fits agree well from pH 4 to 6, although the upward curvatures observed in the CD melts at low temperatures, indicating cold denaturation, were not observed in the DSC data collected at much higher protein concentrations. Similar $\Delta H_{cal}/\Delta H_{vh}$ ratios, ranging from 0.23 to 0.28, were obtained from pH 4 to 6; however, the extent of protein folding decreased substantially below pH 4, and the $\Delta H_{cal}/\Delta H_{vh}$ ratio decreased accordingly. The maximal stability occurred at pH 5, resulting in a $T°$ of 104.5 °C in 0.2 M KCl.

rHMfA was fully folded in 1 M KCl at pH 2 and 3 (Figure 2A), and under these solution conditions, $\Delta H_{cal}/\Delta H_{vh}$ ratios

Table 1: Thermodynamic Parameters of Archaeal Histone Unfolding

			$T°$ (°C)		ΔH_{vh} (kcal/mol)[a]			
histone	[KCl] (M)	pH	DSC	CD	DSC	CD	$\Delta H_{cal}/\Delta H_{vh}$[a]	ΔC_p[a] (cal deg^{-1} mol^{-1})
rHMfA	0.2	3.0	96.1 ± 0.1	84.6 ± 0.1	139.4 ± 0.6	134.1 ± 0.6	0.101 ± 0.001	2102 ± 16
		4.0	97.6 ± 0.1	100.2 ± 0.2	158.3 ± 0.6	161.2 ± 0.8	0.261 ± 0.003	2225 ± 20
		5.0	104.5 ± 0.0	104.1 ± 0.3	164.3 ± 0.3	164.1 ± 1.3	0.227 ± 0.001	2159 ± 37
		6.0	101.0 ± 0.0	101.1 ± 0.2	158.4 ± 0.2	157.3 ± 0.7	0.281 ± 0.001	2178 ± 19
	1.0	2.0		94.0 ± 0.3		136.3 ± 1.2		1867 ± 35
		3.0		100.7 ± 0.2		153.1 ± 1.0		2114 ± 26
		4.0		111.6 ± 0.2		172.1 ± 1.0		2149 ± 27
rHFoB	0.2	4.0	75.6 ± 0.0	*b*	91.1 ± 0.3	*b*	0.501 ± 0.009	*b*
		5.0	76.9 ± 0.0	74.8 ± 0.2	113.5 ± 0.1	115.9 ± 0.1	0.325 ± 0.001	2552 ± 4
		6.0	76.5 ± 0.0	70.9 ± 0.6	94.9 ± 0.1	120.7 ± 2.4	0.673 ± 0.005	2958 ± 92
	1.0	2.0	64.7 ± 0.1	60.3 ± 0.5	114.9 ± 0.4	105.7 ± 1.0	0.091 ± 0.009	1935 ± 17
		3.0	77.0 ± 0.0	73.0 ± 0.2	108.9 ± 0.0	116.0 ± 0.1	0.325 ± 0.001	2332 ± 7
		4.0	90.3 ± 0.0	91.5 ± 0.1	128.6 ± 0.2	125.7 ± 0.4	0.366 ± 0.001	1913 ± 11
		5.0	90.9 ± 0.0	92.0 ± 0.3	124.3 ± 0.2	126.7 ± 0.9	0.330 ± 0.002	1943 ± 25
		6.0	90.5 ± 0.2	87.5 ± 0.2	122.5 ± 0.1	135.7 ± 0.7	0.411 ± 0.001	2381 ± 22
rHMfB	0.2	2.5		78.2 ± 0.1		97.9 ± 0.1		1694 ± 4
		2.7		84.9 ± 0.1		101.1 ± 0.2		1596 ± 5
		3.0		89.3 ± 0.2		112.5 ± 0.5		1713 ± 14
		3.3		94.1 ± 0.1		135.3 ± 0.5		2023 ± 13
		3.7		102.9 ± 0.1		147.8 ± 0.5		2043 ± 11
		4.0		103.4 ± 0.1		145.3 ± 0.5		1975 ± 12
		5.0		112.8 ± 0.3		150.3 ± 0.9		1870 ± 22
		6.0		108.9 ± 0.2		157.6 ± 0.9		2295 ± 21
rHPyA1	0.2	4.0		107.2 ± 0.3		172.2 ± 2.1		2122 ± 90
		5.0		114.1 ± 0.6		184.4 ± 3.0		2389 ± 152
		7.5		109.8 ± 0.3		172.3 ± 1.3		2205 ± 33

[a] The molar unit for the van't Hoff enthalpy and the change in heat capacity upon unfolding is the cooperative unit, i.e., a dimer for the archaeal histones. The values used for the $\Delta H_{cal}/\Delta H_{vh}$ ratio calculations were from DSC data. The errors are standard deviations from the curvature of the χ^2 surface of each fit (*25*) and represent the quality of the fit, not the experimental error. [b] Insufficient baseline information was available between low- and high-temperature denaturations for an adequate fit.

of 0.50 and 0.46 were observed, respectively, consistent with a two-state, dimer unfolding reaction.

(B) rHMfB. As rHMfB unfolded at higher temperatures than rHMfA, complete endotherms could not be obtained by DSC which made obtaining ΔH_{cal} values impossible. The results of representative CD thermal melts at different pHs are shown in Figure 5B, and the thermodynamic parameters derived from fits of the CD data in 0.2 M KCl are listed in Table 1. The $T°$ values obtained for rHMfB were higher than those for rHMfA, whereas the ΔH_{vh} and ΔC_p values were marginally lower. Consistent with rHMfA, the maximal stability for rHMfB was observed at pH 5, resulting in a $T°$ of 113 °C in 0.2 M KCl.

(C) rHPyA1. rHPyA1 was also so stable that complete DSC endotherms could not be obtained. Thermal unfolding transitions were followed by CD, and these were fit well by nonlinear regression, providing a $T°$ of 114 °C in 0.2 M KCl at pH 5 with slightly lower $T°$ values obtained at pH 4 and 7.5 (Table 1). There was no evidence of cold temperature-induced denaturation in CD thermal melts of rHPyA1 (data not shown).

(D) rHFoB. The histone from the mesophile, rHFoB, was partially unfolded under most experimental conditions and exhibited both high- and low-temperature denaturation. Unfolding increased above and below 28 °C in 0.2 M KCl at pH 4−6, and rHFoB was almost completely unfolded at all pHs below pH 4 and at all temperatures below 10 °C (Figure 6A). Maximal folding in 0.2 M KCl, ∼35% of the potential maximum, was observed at pH ∼5. This resulted in a $T°$ of 75 °C, and under these conditions, a 1 mM rHFoB solution would exhibit 5−7% unfolding between 20 and 40

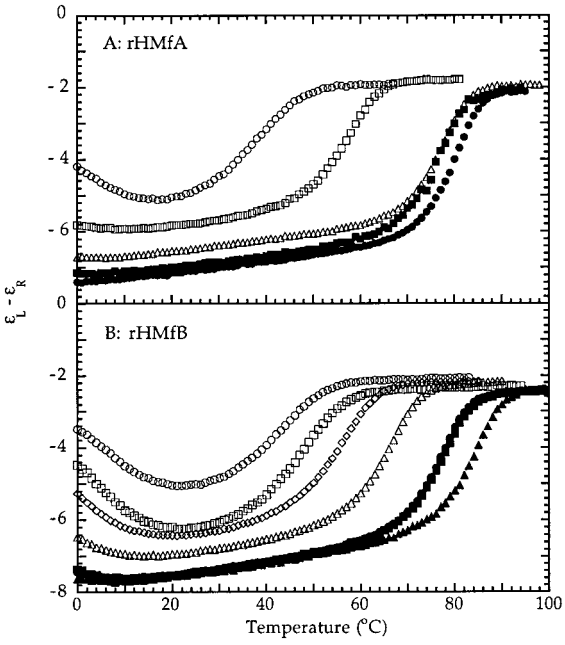

FIGURE 5: pH dependency of the thermal unfolding of rHMfA and rHMfB in 0.2 M KCl followed by CD. (A) rHMfA concentrations were 3.3 μM at pH 2 in 25 mM glycine buffer (○), 3.7 μM at pH 3 in 25 mM glycine buffer (□), 2.3 μM at pH 4 in 25 mM glycine buffer (△), 2.4 μM at pH 5 in 25 mM acetate buffer (●), and 2.5 μM at pH 6 in 25 mM MES buffer (■). (B) rHMfB concentrations were 5.1 μM at pH 2.5 in 25 mM glycine buffer (○), 3.3 μM at pH 2.7 in 25 mM glycine buffer (□), 4.5 μM at pH 3 in 25 mM glycine buffer (◇), 4.1 μM at pH 3.3 in 25 mM glycine buffer (△), 4.6 μM at pH 3.7 in 25 mM glycine buffer (●), 4.4 μM at pH 4 in 25 mM glycine buffer (■), and 2.4 μM at pH 5 in 25 mM acetate buffer (▲).

Table 2: Thermodynamic Parameters for Archaeal Histone Stability[a]

	rHFoB	rHMfA	rHMfB	rHPyA1
$\Delta G°_{max}$ (kcal/mol)	7.2	15.5	14.6	17.2
T_{max} (°C)	32	35	40	44
$\Delta G°$ at the growth temperature (kcal/mol)	6.8 (43 °C)[b]	7.8 (83 °C)	9.4 (83 °C)	8.0 (95 °C)
$T°$ (°C)	74.8	104.0	112.8	114.1

[a] Values based on the stability curves shown in Figure 8. [b] Optimum growth temperature of the archaeon from which the histone originates.

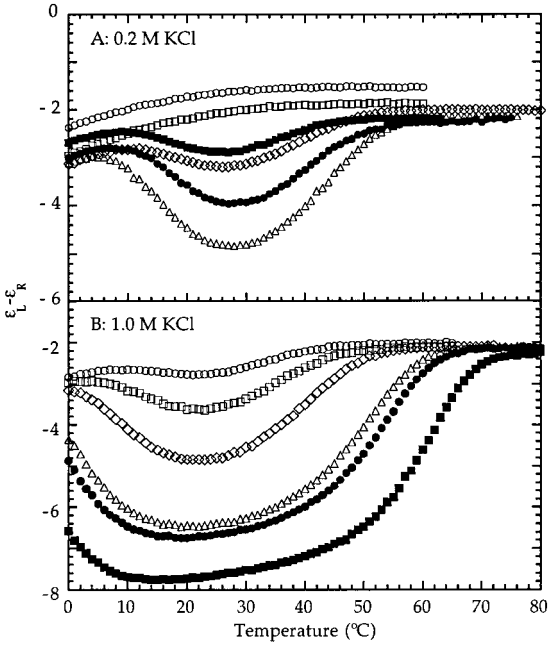

FIGURE 6: Salt and pH dependency of thermal unfolding of rHFoB followed by CD. (A) Unfolding in 0.2 M KCl of rHFoB solutions that were 5.7 μM at pH 2 in 25 mM glycine buffer (○), 4.4 μM at pH 3 in 25 mM glycine buffer (□), 4.5 μM at pH 4 in 25 mM glycine buffer (◇), 4.7 μM at pH 5 in 25 mM acetate buffer (△), 4.2 μM at pH 6 in 25 mM MES buffer (●), and 4.4 μM at pH 7.5 in 25 mM phosphate buffer (■). (B) Unfolding in 1 M KCl and 25 mM glycine buffer of rHFoB solutions that were 4 μM at pH 2 (○), 3.4 μM at pH 2.6 (□), 3.4 μM at pH 2.7 (◇), 3.4 μM at pH 3.3 (△), 3.5 μM at pH 3.5 (●), and 3.7 μM at pH 4.1 (■).

°C. Because of the lower stability of rHFoB, it was also possible to observe complete CD and DSC transition data in 1 M KCl with well-defined pre- and post-transition baselines. rHFoB was ~95% folded at 20 °C in 1 M KCl at pH 4 but exhibited a reduced maximal extent of folding and a substantial decrease in thermostability below pH 4 (Figure 6B). The results of fitting the DSC and CD data collected for rHFoB from pH 2 to 6 in 0.2 and 1 M KCl are listed in Table 1. As indicated, consistent thermodynamic parameters were obtained by fits of the two-state, dimer unfolding model to the data generated by the two methods.

DISCUSSION

The availability of a large number of naturally occurring archaeal histones, with very similar amino acid sequences (Figure 1) but substantially different stabilities (Tables 1 and 2), offers a tractable experimental system for elucidating structure−stability relationships. Cross-linking and NMR studies have established that the archaeal histones are dimers in solution (*4*, *5*, *8*), and here we have shown that thermal unfolding data generated for four archaeal histones are fit well by a two-state model in which a dimer unfolds directly to two random coils, as previously established for unfolding

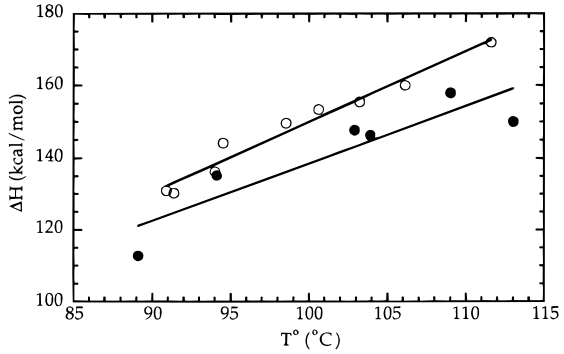

FIGURE 7: Temperature dependency of the enthalpy of unfolding of rHMfA (○) and rHMfB (●) in 0.2 M KCl derived from CD data collected from pH 3 to 7.5. A linear least-squares fit of the $\Delta H°_{vh}$ vs $T°$ plot provides a ΔC_p of 1950 cal deg^{-1} (mol of dimer)$^{-1}$ for rHMfA and 1593 cal deg^{-1} (mol of dimer)$^{-1}$ for rHMfB.

of eukaryal histones (*26*, *27*). As predicted for dimers, thermal unfolding transitions observed by CD and DSC were asymmetric and concentration-dependent, and the ability to fit both of these attributes with the dimer unfolding model is outstanding. Discrepancies exist between the predicted and measured $\Delta H_{cal}/\Delta H_{vh}$ ratios; however, these are reasonably attributed to errors in the ΔH_{cal} values that resulted from inaccuracies in defining post-transition baselines. The baseline information available following the high-temperature unfolding of the histones from hyperthermophiles was frequently insufficient for a reliable fit.

Changes in Heat Capacity (ΔC_p) upon Unfolding. The ΔC_p for protein unfolding controls the curvature of the protein stability curve, and is potentially an important parameter in controlling thermal stability (*24*, *28*, *29*). The ΔC_p during unfolding is thought to result largely from changes in the hydration of hydrophobic residues, and Murphy and Freire (*30*) have proposed that $\Delta C_p = 0.45\Delta ASA_{ap} - 0.26\Delta ASA_{pol}$, in which ΔASA_{ap} and ΔASA_{pol} are the changes that result from protein unfolding in the solvent accessible surface areas of apolar and polar groups, respectively.

The structure of rHMfB (*4*) predicts a ΔASA_{ap} of 6398.5 Å^2 and a ΔASA_{pol} of 4344.7 Å^2 during rHMfB unfolding, from which the Murphy−Freire equation (*30*) gives a ΔC_p of 1750 cal deg^{-1} (mol of dimer) $^{-1}$ or 12.7 cal deg^{-1} residue^{-1}. The average ΔC_p determined experimentally for rHMfB from CD thermal melts at pH 3−6 in 0.2 M KCl is 1986 ± 194 cal deg^{-1} (mol of dimer) $^{-1}$ or 13.8 cal deg^{-1} residue^{-1} [69 residues per monomer (Table 1)], whereas a Kirchhoff plot of ΔH_{vh} versus $T°$ based on these data gives a ΔC_p of 1593 ± 174 cal deg^{-1} (mol of dimer)$^{-1}$ or 13 cal deg^{-1} residue^{-1} (Figure 7). These two experimentally defined ΔC_ps therefore flank the ΔC_p value predicted for rHMfB by the Murphy−Freire equation. Although the difference between the experimental ΔC_p values is only slightly larger than the error in their measurements, a similar

difference was also observed for ΔC_p values measured for Sac7d, an unrelated archaeal DNA-binding protein from the thermophile *Sulfolobus acidocaldarius.* This difference could be explained by the linkage of protonation and anion binding to protein folding (*24*). The average ΔC_p values determined from the data in Table 1 for rHFoB, rHMfA, and rHPyA1 are 2101 ± 234, 2166 ± 51, and 2239 ± 137 cal deg^{-1} (mol of dimer)$^{-1}$ or 15.7, 15.9, and 16.7 cal deg^{-1} residue^{-1} , respectively, and a Kirchhoff plot of the CD data for rHMfA again gives a lower ΔC_p of 1950 ± 34 cal deg^{-1} (mol of dimer)$^{-1}$ or 14.3 cal deg^{-1} residue^{-1} (Figure 7). The archaeal histones do not therefore appear to have very different ΔC_ps during unfolding, and have ΔC_p values for unfolding that are similar to those reported for other globular proteins from mesophiles, e.g., 12.4 cal deg^{-1} residue^{-1} for the protein G IgG binding domain (*31*), 11.9 cal deg^{-1} residue^{-1} for ubiquitin (*32*), 11.3 cal deg^{-1} residue^{-1} for ribonuclease A (*33*), 11.1 cal deg^{-1} residue^{-1} for spectrin SH3 (*34*), and 13.1 cal deg^{-1} residue^{-1} for HPr (*35*).

pH and Salt Dependency of Thermostability. The thermostability of the archaeal histones decreases progressively below pH 4, a behavior common to many proteins due to the linkage of protonation of carboxyl side chains to the folding reaction. Protonation increases positive charge density in regions involved in structure stabilization and may eliminate stabilizing salt bridges (*24*, *36*−*40*). Salt addition can screen potentially repulsive charge interactions, can promote anion binding at sites previously occupied by carboxyl groups, and may also stabilize hydrophobic interactions (*24*, *38*, *39*, *41*, *42*). Interestingly, the thermostability of the archaeal histones decreased above pH 5, most likely as a result of deprotonation of histidine 49 (H49), the only histidine present in these four proteins (Figure 1). Deprotonation of H49 may remove a stabilizing salt bridge and/or increase the overall hydrophobicity of the histone core.

Salt-promoted refolding, particularly at low pH, suggests a linkage between anion binding and protein folding, and a plot of the ln K_{app} (the apparent equilibrium constant for renaturation) versus the ln[KCl] yields a straight line. The slope of this line provides an apparent stoichiometry for anion binding, and although the molecular explanation of this parameter remains unclear, it seems noteworthy that such plots for rHMfA and rHMfB yielded slopes of ∼3 (*8*) whereas the data for rHFoB yield a slope of ∼6. The order of the effectiveness of salt in promoting archaeal histone folding at pH 2 (Figure 2A) correlates with the order of their maximal stabilities (Table 2), as expected from a consideration of the effects of linkage of anion binding to protein stability (*40*). The influence of salt on the extent of folding is thus most pronounced, and the largest change in folding is observed for the least stable protein, rHFoB. In contrast, rHPyA1 is so stable that changing the salt environment had no measurable effect on the extent of folding at pH 2. This does not necessarily mean that salt has no effect on the stability of the rHPyA1 fold, but only that such effects were not discernible in vitro using the experimental approaches and conditions of this study.

Protein Stability Curves. For comparative purposes, the influence of concentration on protein stability can be avoided by considering $T°$ and $\Delta G°$ values, and stability curves, $\Delta G°$ versus temperature (*29*), are shown in Figure 8 for the archaeal histones in 0.2 M KCl at pH 5. The maximal

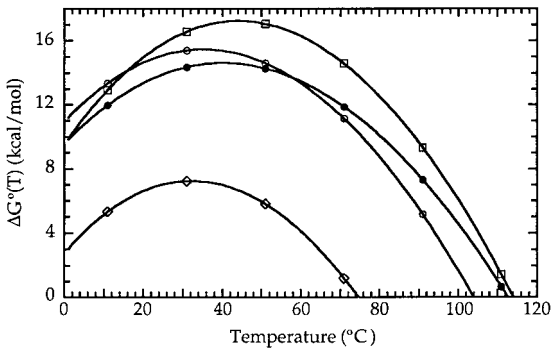

FIGURE 8: Protein stability curves for rHPyA1 (□), rHMfA (○), rHMfB (●), and rHFoB (◇) at pH 5 in 0.2 M KCl.

stabilities of rHFoB, rHMfA, rHMfB, and rHPyA1 occur at 32, 35, 40, and 44 °C, respectively, and there is a 10 kcal/mol difference between the maximal stabilities of rHFoB and rHPyA1, the least and most stable histones, respectively. There is however only a 1.2 kcal/mol difference between their stabilities at the optimum growth temperatures of the originating *Archaea* (Table 2). The $T°$ values for rHFoB, rHMfA, rHMfB, and rHPyA1 are 75, 104, 113, and 114 °C, respectively, at pH 5 in 0.2 M KCl, a 39 °C range in thermostability for four ancestrally homologous proteins that retain the same fold and have sequences that are 75−90% identical (Figure 1). To our knowledge, this is only the second quantitative comparison of the thermodynamic stabilities of homologous proteins from mesophiles and thermophiles. Nojima et al. (*28*) reported previously that the structures of cytochrome *c*-552 and phosphoglycerate kinase from *Thermus thermophilus* were 15 and 4 kcal/mol more stable, respectively, than their homologues from mesophiles.

Basis for the Differences in Archaeal Histone Stabilities. The sequences of rHFoB, rHMfA, rHMfB, and rHPyA1 are aligned in Figure 1 together with the sequences of 14 additional archaeal histones (*1*). Nineteen positions (28%) contain the same residue in all the archaeal histones, and an additional 16 positions (23%) are filled by one of two residues. However, there are five different residues at positions 25, 26, 31, 37, 38, and 64, six at positions 35 and 41, seven at position 27, and eight at position 66 which is also the C-terminal residue in eight histones. With one exception, asparagine 14 (N14) in rHMfA, asparagine residues that could suffer deamination at high temperatures are not present in the histones from hyperthermophiles but do occur in the HFo histones from the mesophile *M. formicicum* and in the HMt histones from the moderate thermophile *Methanobacterium thermoautotrophicum* (Figure 1). In contrast, bulky phenylalanine and tyrosine residues that could increase the packing and reduce the overall flexibility are present in the histones from hyperthermophiles but are not present in the HFo and HMt histones.

Comparing the rHMfB (*4*) and rHFoB (*5*) structures suggests that the presence of arginine 37 (R37) in rHMfB versus glutamate 37 (E37) in rHFoB may contribute to the higher stability and lower salt dependency of the rHMfB fold. These are surface residues, and in rHMfB, R37 can form favorable ionic interactions with glutamate 33 (E33) along the exposed surface of α-helix 2 and with aspartate 14 (D14) in α-helix 1 of the partner polypeptide in a rHMfB dimer. In contrast, in rHFoB, there is the potential for a repulsive E33−E37 interaction, which presumably requires salt screen-

ing, and the α-helix 1−α-helix 2 interaction is a less favorable N14−E37. Comparing the residues at positions 14, 34, and 37 in the other archaeal histones (Figure 1) does not however add support to these ionic interactions playing a consistent role in determining archaeal histone stabilities. rHMfA has a stability similar to that of rHMfB and is less salt-dependent (Figure 2A and Tables 1 and 2); however, rHMfA has the same residues at positions 14, 34, and 37 as rHFoB, and hydrophobic residues occupy position 37 in all the other histones from hyperthermophiles, eliminating the opportunity for ionic interactions.

Analysis of the hydrophobic cores of the rHMfB and rHFoB structures reveals that there is a cavity adjacent to glycine 36 (G36) that is larger and more solvent accessible in rHFoB than in rHMfB (*4*, *5*). This cavity is bounded and partially filled by the side chains of the residues at positions 31, 35, and 64 which, as noted above, are all positions that exhibit high levels of residue variability. On the basis of the alignment in Figure 1, the combination of alanine 31 (A31) and valine 64 (V64) in rHFoB is the second smallest in terms of space filling, and rHFoB has a potentially polar lysine residue at position 35 (K35). Consistent with the size and hydrophobicity of the residue at positions 31 and 35 being important for stability, variants of rHFoB constructed with A31I and K35M substitutions unfold at temperatures that are 11 and 14 °C higher, respectively, than that of wild-type rHFoB, and the reciprocal I31A and M35K variants of rHMfB unfold at temperatures that are 4 and 17 °C lower, respectively, than that of wild-type rHMfB (W.-t. Li and J. N. Reeve, unpublished results). As revealed by the alignment, most of the histones from hyperthermophiles have at least two of these positions filled by large hydrophobic residues and several also have a larger alanine 36 in place of G36.

Thermostability in Vivo. As the archaeal histones are dimers in solution, the temperatures at which they unfold are concentration-dependent (Figure 4), and their thermostabilities in vivo must therefore depend on their intracellular concentrations. The stability of a protein with a concentration-dependent T_m is given by

$$\Delta G_m(T) = \Delta H_m\left(\frac{T_m - T}{T_m}\right) - (T_m - T)\Delta C_p + T\Delta C_p \ln\left(\frac{T_m}{T}\right) \quad (11)$$

where

$$\Delta H_m = \Delta H^\circ + \Delta C_p(T_m - T^\circ) \quad (12)$$

On this basis, the effects of concentration on both the extent of folding and the free energy of unfolding are shown in panels A and B of Figure 9 for a protein with a ΔH° of 150 kcal/mol, a T° of 110 °C, and a ΔC_p of 2000 cal deg^{-1} mol^{-1}, i.e., thermodynamic parameters representative of those established here for the archaeal histones from hyperthermophiles. At concentrations below 1 mM, as might be expected in vivo, this protein would be largely unfolded above 100 °C, and at 1 mM would be ∼10% unfolded at 85 °C (panels A and B of Figure 9). The possibility of such marginal stability in vivo has similarly been predicted for Sac7d (*24*, *40*), and although both Sac7d and the histones

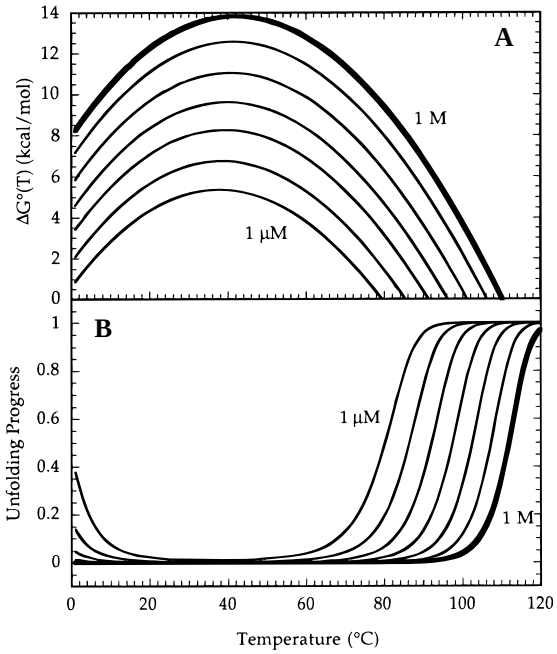

FIGURE 9: (A) Protein stability curves, as a function of protein concentration at pH 5 in 0.2 M KCl, for a hypothetical protein with a ΔH°_{vh} of 150 kcal/mol, a T° of 110 °C, and a ΔC_p of 2000 cal deg^{-1} (mol of dimer)$^{-1}$. The curves show the stabilities predicted for protein solutions ranging from 1 μM to 1 M protein (heavy line), each interval representing a 10-fold increase in protein concentration. (B) Unfolding progress, as a function of temperature, for the hypothetical protein at 1 μM to 1 M protein concentrations.

may be stabilized by DNA binding, this would reduce the effective concentration of free protein in the cytoplasm, and shift the stability curve of the free protein to an even lower temperature. Although it is unlikely that there is a large pool of free histone in vivo (*43*), a significant portion of this pool may therefore be unfolded.

The cytoplasm of *Me. fervidus* cells contains ∼1 M K^+ (*44*), and consistent with this, the structures of rHMfA and rHMfB require relatively high KCl concentrations for maximal stability (Figure 2A). On the basis of data from close relatives, *M. formicicum* and *Pyrococcus* GB-3a similarly are likely to contain ∼300 and ∼600 mM K^+, respectively (*44*, *45*); however, rHFoB required higher KCl concentrations than rHMfA and rHMfB for maximal stability, whereas salt had no discernible effect on the folded structure of rHPyA1 in vitro (Figure 2A). As discussed above, salt still may play a role in rHPyA1 stability, particularly in vivo if the concentration of HPyA1 free in the cytoplasm of *Pyrococcus* cells growing at 95 °C is very low.

Thermodynamic Stability, Thermostability, and Targets for Mutagenesis. The stability curves in Figure 8 demonstrate that there are inherent quantitative differences in the thermodynamic stabilities of the archaeal histones, which result in different thermal stabilities compared as T° values (Table 2). By site-specific mutagenesis, combined with CD and DSC assays of the resulting variants, it should be possible to identify the residues and interactions that contribute substantially to these differences, with the alignment in Figure 1 providing directions to increased or decreased stability. It should also be possible to identify the residues and interactions that are responsible for the different salt dependencies of the archaeal histone folds. Frequently in thermostability studies, an enzyme is incubated at a high

temperature and the residual activity is then assayed after increasing times at the high temperature. Using this approach, the HFo histones lost DNA binding and compacting activities faster than rHMfA and rHMfB when they were incubated at 90 °C, although rHMfA and rHMfB did eventually lose activity at 90 °C, whereas rHPyA1 retained full activity even after 60 h at 90 °C (*12*, *46*). These are also stability differences that can be dissected by reverse genetics, and for the archaeal histones, it should be possible to separate stability as documented here in thermodynamic terms from heat resistance defined by the kinetics of functional inactivation.

REFERENCES

1. Reeve, J. N., Sandman, K., and Daniels, C. J. (1997) *Cell 89*, 999−1002.
2. Arents, G., and Moudrianakis, E. N. (1995) *Proc. Natl. Acad. Sci. U.S.A. 92*, 11170−11174.
3. Ramakrishnan, V. (1995) *Proc. Natl. Acad. Sci. U.S.A. 92*, 11328−11330.
4. Starich, M. R., Sandman, K., Reeve, J. N., and Summers, M. F. (1996) *J. Mol. Biol. 255*, 187−203.
5. Zhu, W., Sandman, K., Lee, G. E., Reeve, J. N., and Summers, M. F. (1998) *Biochemistry 37*, 10573−10580.
6. Sandman, K., Krzycki, J. A., Dobrinski, B., Lurz, R., and Reeve, J. N. (1990) *Proc. Natl. Acad. Sci. U.S.A. 87*, 5788−5791.
7. Grayling, R. A., Sandman, K., and Reeve, J. N. (1994) *Syst. Appl. Microbiol. 16*, 582−590.
8. Grayling, R. A., Becktel, W. J., and Reeve, J. N. (1995) *Biochemistry 34*, 8441−8448.
9. Sandman, K., Grayling, R. A., Dobrinski, B., Lurz, R., and Reeve, J. N. (1994) *Proc. Natl. Acad. Sci. U.S.A. 91*, 12624−12628.
10. Sandman, K., Grayling, R. A., and Reeve, J. N. (1995) *BioTechnology 13*, 504−506.
11. Sandman, K., Perler, F. B., and Reeve, J. N. (1994) *Gene 150*, 207−208.
12. Darcy, T. J., Sandman, K., and Reeve, J. N. (1995) *J. Bacteriol. 177*, 858−860.
13. Sambrook, J., Fritsch, E. F., and Maniatis, T. (1989) *Molecular cloning: a laboratory manual*, Cold Spring Harbor Laboratory Press, Cold Spring Harbor, NY.
14. Peränen, J., Rikkonen, M., Hyvönen, M., and Kääriäinen, L. (1996) *Anal. Biochem. 236*, 371−373.
15. Deutscher, M. P. (1990) *Methods Enzymol. 182*, 62−63.
16. Steif, C., Weber, P., Hinz, H.-J., Flossdorf, J., Cesareni, G., and Kokkinidis, M. (1993) *Biochemistry 32*, 3867−3876.
17. Thompson, K. S., Vinson, C. R., and Freire, E. (1993) *Biochemistry 32*, 5491−5496.
18. Marky, L. A., and Breslauer, K. J. (1987) *Biopolymers 26*, 1601−1620.
19. Freire, E., and Biltonen, R. (1978) *Biopolymers 17*, 463−479.
20. Privalov, P., and Potekhin, S. A. (1986) *Methods Enzymol. 131*, 4−51.
21. Freire, E. (1989) *Comm. Mol. Cell. Biophys. 6*, 123−140.
22. Freire, E. (1995) *Methods Enzymol. 259*, 144−168.
23. Privalov, P. (1979) *Adv. Protein Chem. 33*, 167−241.
24. McCrary, B. S., Edmondson, S. P., and Shriver, J. W. (1996) *J. Mol. Biol. 264*, 784−805.
25. Bevington, P. R. (1969) *Data reduction and error analysis for the physical sciences*, McGraw-Hill, New York.
26. Karantza, V., Baxevanis, A. D., Freire, E., and Moudrianakis, E. N. (1995) *Biochemistry 34*, 5988−5996.
27. Karantza, V., Freire, E., and Moudrianakis, E. N. (1996) *Biochemistry 35*, 2037−2046.
28. Nojima, H., Ikai, A., Oshima, T., and Noda, H. (1977) *J. Mol. Biol. 116*, 429−441.
29. Becktel, W. J., and Schellman, J. A. (1987) *Biopolymers 26*, 1862−1877.
30. Murphy, K. P., and Freire, E. (1992) *Adv. Protein Chem. 43*, 313−361.
31. Alexander, P., Fahnestock, S., Lee, T., Orban, J., and Bryan, P. (1992) *Biochemistry 31*, 3597−3603.
32. Wintrode, P. L., Makhatadze, G. I., and Privalov, P. (1994) *Proteins 18*, 246−253.
33. Privalov, P., and Khechinashvili, N. (1974) *J. Mol. Biol. 86*, 665−684.
34. Viguera, A. R., Martinez, J. C., Filimonov, V. V., Mateo, P. L., and Serrano, L. (1994) *Biochemistry 33*, 2142−2150.
35. Scholtz, J. M. (1995) *Protein Sci. 4*, 35−43.
36. Matthew, J. B., Gurd, F. R. N., Garcia-Moreno, B., Flanagan, M. A., March, K. L., and Shire, S. J. (1985) *CRC Crit. Rev. Biochem. 18*, 91−197.
37. Yang, A. S., and Honig, B. (1993) *J. Mol. Biol. 231*, 459−474.
38. Garcia-Moreno, B. (1994) *Methods Enzymol. 240*, 645−667.
39. Garcia-Moreno, B. (1995) *Methods Enzymol. 259*, 512−538.
40. McCrary, B. S., Bedell, J., Edmondson, S. P., and Shriver, J. W. (1998) *J. Mol. Biol. 276*, 203−224.
41. Fink, A., Calciano, L., Goto, Y., Kurotsu, T., and Palleros, D. (1994) *Biochemistry 33*, 12504−12511.
42. Makhatadze, G., Lopez, M. M., Richardson, J. M., III, and Thomas, S. (1998*) Protein Sci. 7*, 689−697.
43. Pereira, S. L., Grayling, R. A., Lurz, R., and Reeve, J. N. (1997) *Proc. Natl. Acad. Sci. U.S.A. 94*, 12633−12637.
44. Hensel, R., and König, H. (1988) *FEMS Microbiol. Lett. 49*, 75−79.
45. Scholz, S., Sonnenbichler, J., Schäfer, W., and Hensel, R. (1992) *FEBS Lett. 306*, 239−242.
46. Soares, D., Dahlke, I., Li, W.-T., Sandman, K., Hethke, C., Thomm, M., and Reeve, J. N. (1998) *Extremophiles 2*, 75−81.

BI973006I